Acta Oceanol. Sin., 2014, Vol. 33, No. 11, P. 155–160
DOI: 10.1007/s13131-014-0565-8
http://www.hyxb.org.cn
E-mail: hyxbe@263.net

A continental slope stability evaluation in the Zhujiang River Mouth Basin in the South China Sea

LIU Ke[1,2,3]*, WANG Jianhua[1,2]

[1] State Key Laboratory of Hydraulic Engineering Simulation and Safety, Tianjin University, Tianjin 300072, China
[2] Geotechnical Engineering Institute, Tianjin University, Tianjin 300072, China
[3] College of Mining Engineering, Hebei United University, Tangshan 063009, China

Received 8 October 2013; accepted 17 June 2014

Abstract

In nature, a slope stability is determined by the ratio of a sliding resistance to a slide force. The slide force of a marine deep-water continental slope is mainly affected by sediment mechanics properties, a topography, and a marine seismic. However, the sliding resistance is mainly affected by sedimentary patterns and a sedimentary stress history. Both of these are different from case to case, and their impact can be addressed when the data are organized in a geographic information system (GIS). The study area on the continental slope in Zhujiang River Mouth Basin in South China Sea provides an excellent opportunity to apply GIS spatial analysis technology for the evaluation of the slope stability. In this area, a continental slope topography and a three-dimension (3-D) topography mapping show a sea-floor morphology and the distribution of a slope steepness in good detail, and the sediment analysis of seabed samples and an indoor appraisal reveals the variability of a sediment density near the sea-floor surface. On the basis of the results of nine geotechnical studies of submarine study areas, it has worked out that an equivalent cyclic shear stress ratio is roughly between 0.158 and 0.933, which is mainly depending on the initial water content of sediment. A regional density, slope and level of anticipated seismic shaking information are combined in a GIS framework to yield a map that illustrates a continental slope stability zoning under the influencing factors in Zhujiang River Mouth Basin in the South China Sea. The continental slope stability evaluation can contribute to north resources development in the South China Sea, the marine functional zoning, the marine engineering construction and adjust measures to local conditions, at the same time also can provide references for other deep-water slope stability analysis.

Key words: South China Sea, continental slope stability, geographic information system, evaluation

Citation: Liu Ke, Wang Jianhua. 2014. A continental slope stability evaluation in the Zhujiang River Mouth Basin in the South China Sea. Acta Oceanologica Sinica, 33(11): 155–160, doi: 10.1007/s13131-014-0565-8

1 Introduction

Large-scale marine deep-water continental slope consists of loose and thick sediments which are wide distributed, so the ocean continental slope stability evaluation is down to the sea-floor sediment stability evaluation. In general, the relative values of a sliding resistance in the seabed sediment and the driving force determine the stability of a submarine slope. However, determining the glide driving force and anti-sliding force of a large continental slope body still has many difficulties in the actual operation because many deep-penetration samples need to be taken and an extensive set of sophisticated geotechnical tests need to be performed on the samples in order to comprehensively assess a failure potential (Lee et al.,1999).

Some researchers have studied the development characteristics of north continental slope and geological disasters in Zhujiang River Mouth Basin (Maslin et al., 1998; Rothwell et al., 1998; Song, 2003; Wu et al., 2008). Neither of these previous studies took advantage of the capabilities of the modern geographic information systems (GIS), which can combine detailed sets of regional data to yield predictive maps of quantities such as the potential for slope failure. This paper has summarized main influence factors which lead to the slope failure, including the substrate types and their physical and mechanical properties, topography characteristics and earthquake action. This article has applied them within the framework of the GIS to the stability evaluation in the Zhujiang River Mouth Basin.

2 Site background

The South China Sea is one of the largest marginal seas in the western Pacific area, covering about 3×10^6 km^2, belonging to a part of the basin systems in the western Pacific edge grooves and arcs. The shelf, the slope and the deep sea basin in the South China Sea are vast, and there are many islands, reefs, sea platforms, basins, seamounts and trenches (Liu and Liu, 2005). The north continental slope is located to south of southeast China Mainland and to west of Taiwan Island, about 900 km long, and it is distributed from NE to SW direction, similar to the RUYI shape, as a whole flat and broad. The Dongsha Islands lie in it (Fig. 1).

The study area is in Zhujiang River Mouth Basin in South China Sea, located in 18°–22°N, 110°–120°E, 160–240 km to southeast of Hong Kong, the water depth 300–3 000 m (Fig. 2), where an oil and a gas are rich. A submarine complex geological structure and a sedimentary history lead to the complicated

*Corresponding author, E-mail: liuke1976@163.com

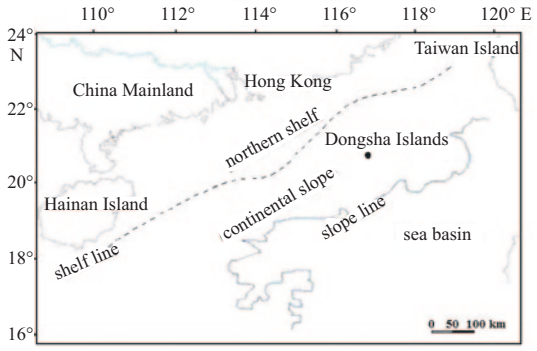

Fig.1. Location of northern continental slope in South China Sea (Liu and Liu, 2005).

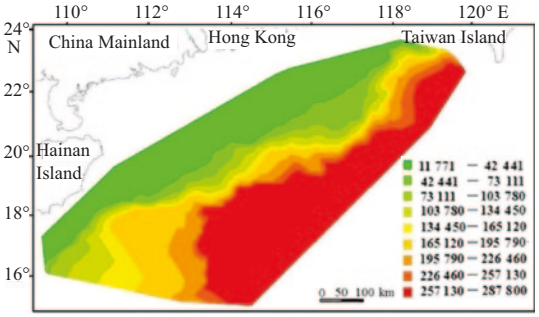

Fig.2. 3-D topography (cm) of northern continental slope.

topography and geomorphology features, where a slump and a variety of hazardous geological factors easily emerge.

3 Continental slope stability analysis in Zhujiang River Mouth Basin

3.1 *Some assumptions in producing the present GIS slope stability map*

The development of a continental slope stability map required the following series of assumptions that limit the applicability of the figure.

(1) Deposits will not change with depth in the sedimentary section. Sediment particles are same as sample points.

(2) The normal consolidation soil is under about 2.5 m in sedimentary profile. The over consolidated and under consolidation state are not considered.

(3) The unstability of the slope caused by the groundwater activities is not taken into account.

(4) The slope steepness of seabed changes uniformly, infinite slope.

(5) In the cyclic shear, deposits are fine grained sediment characteristics.

If we have additional data, the above assumptions can be changed. For example, if we have the deep drilling sediment samples, especially a lot of seismic data, we can improve the evaluation on the mechanical behavior of deeper soil. The under consolidation state can be determined by a pore water pressure test in site and consolidation test of deep drilling sediment sample and the permeability of water can also be determined by the pore water pressure. The over consolidated sediment can be determined by the equation of Lee and Edwards (1986).

3.2 *Driving force assessment*

Lee and Edwards (1986) put forward to evaluate a slope slide force using three elements: (1) gravity force; (2) the seismic load; and (3) the wave load. Lambe and Whitman (1969) pointed out an excess pore water pressure related to a penetration could be used as a driving force or as a part of lower strength mechanics. In this paper, the penetration is a lower intensity factor rather than the driving force.

The gravity is always considered as a constant force in the stability analysis. Because the water depth around the continental slope of the South China Sea is between 300 and 3 000 m, the wave load need not be considered. According to Morgenstern (1967) modifying seismic load equation, the expression is as follows:

$$\tau_s / \gamma' h = k(\gamma / \gamma') + \sin\alpha, \quad (1)$$

where τ_s is the slope shear stress caused by the earthquake; $\gamma' h$ is the product of the buoyant unit mass and depth in the sediment column; k is a horizontal seismic acceleration; γ / γ' is the ratio of total to buoyant sediment unit mass; and α is a continental slope angle.

The submarine topography in the study area begins from a low water line, crosses a gentle shelf, a shelf line, and a continental slope (where the water depth increases quickly and the continental slope is complex) into the flat terrain of deep sea basin.

By the relief size about the points of the pattern, 40 slope controlled points have been selected to analyze the slope steepness (Fig. 3). The slope gradients at controlled points are between 0.027 and 5.579. On the basis of the above data, this paper used the Arc/Info SLOPE function to construct the bottom SLOPE figure (Fig. 4). The bottom slope figure comes into an environmental load condition which leads to the slope instability.

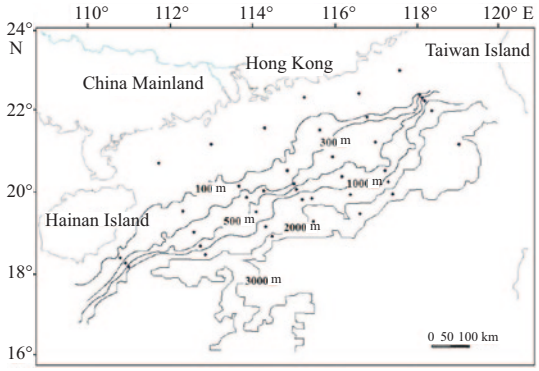

Fig.3. Water-depth contours and grade controlled points (Liu and Liu, 2005).

According to the slope steepness, the study area can be classified as nine color areas. A minimum value of the slope steepness 0.027 and the maximum value 5.579. The color shades

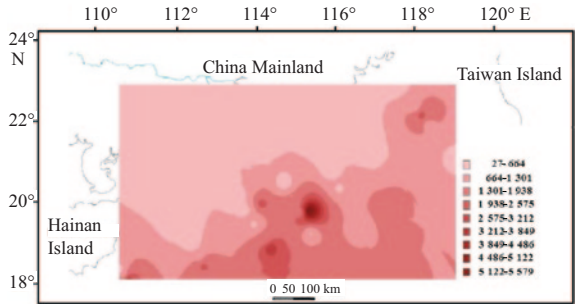

Fig.4. GIS continental slope gradient [(1/1 000)°] map.

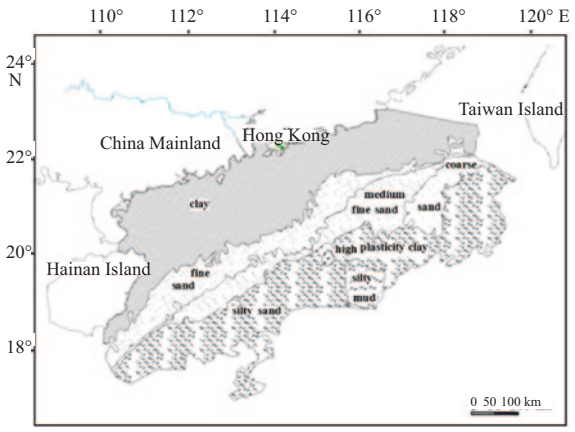

Fig.5. Seabed sediments distribution (Liu and Liu,2005; Luan et al.,2009; Luan et al.,2010; Zhang et al.,2010; Zou et al.,2012).

reflecting slope gradient value, the deep color is representative of the bigger value. On the contrary, the light color is representative of the small angle. In addition, Fig. 4 shows that the whole formation of the northern continental slope is extremely irregular and the morphology fiercely changes from northwest to southeast.

On the basis of the slope terrain change, the slope from top to bottom can be divided into three sections:

(1) The upper slope is on the northwest of the continental slope, north of 20°30'N, and in the vicinity of 118°E, and the bottom slope angle is bigger, where the slope value is up to 1.938;

(2) The middle slope is in the west area of 118°E, gentle terrain, slope gradient only 1.301, the slope relatively flat;

(3) The lower slope has long submarine canyons which show SN direction, near 20°N and 115°E, where the terrain changes fiercely, and the slope value is up to 5.579.

3.3 *Sediment types with their physical and mechanical indexes*

On the basis of the seabed samples, the indoor appraisal analysis (Table 1) and previous works (Liu and Liu, 2005; Luan et al., 2009; Luan et al., 2010; Zhang et al., 2010; Zou et al., 2012), this paper has found that the substances of surface sediments are mainly terrigenous clastic accumulation and particles are fine. In the study area, seabed sediments can be classified into seven types: clay, fine sand, medium-fine sand, coarse sand, high plastic clay, silty sand and silty mud.

Clay is widespread in the sea bottom, accounting for roughly 30% of the total area, mainly in the shallow-water region along China's Mainland coast, 100 m depth contour position. From north to south, at 200 m depth contour position the majority sediment is fine sand, accounting for about 15% of the study area, and farther south to about 1 000 m depth contour the medium-fine sand accounts for about 15% of the study area. Coarse sand is less distributed at the Dongsha Islands Bottom Plateau. Silty sand is distributed between 500 and 3 000 m depth contour accounting for about 30%. High plastic clay is mainly distributed in the Dongsha Islands Submarine Canyon with N-W direction and the Liwan Submarine Canyon with S-N direction. Because of the continental shelf sediments or sliding slope deposition at the continental slope toe, a huge continental turbidity body leads to the bottom continental rise (mainly silty mud, distribution area between 2 500 and 3 000 m depth). The whole slope area of sediment presents roughly the banded distribution along N-E direction (Fig. 5).

The northern shelf of the South China Sea begins from the coastal shallow inland, passing through the outside shelf to the slop, and the seabed sediment particle size increases gradually. It shows that sedimentary characteristic law of the seabed deposition is contrary to the general.

The bulk density of the seabed sediment in Zhujiang River Mouth Basin is at 10 cm depth, and the marine sediment bulk density can be as a layer in the GIS (Fig. 6). First, considering the disturbance of the marine biological activity (Alexander and Simoneau, 1999); Second, the 10 cm depth representing the natural state of recently deposited soils, no need to revise a consolidation state, so this paper selects the 10 cm depth.

The ratio (γ'/γ) of mean buoyant unit mass to mean total unit one in the sea bottom cannot be established on the bulk density of 10 cm depth. Reason is that the sediment consolidation state cannot represent a deeper soil consolidation in such a shallow sea bottom. In order to get more representative value of

Table 1. Zhujiang River Mouth Basin marine sediment physical and mechanical indexes

Sediment type	Water content/%	Bulk density /g·cm^{-3}	Void ratio	Relative density	Buoyant density/g·cm^{-3}
Clay	113.00	1.62	3.48	2.65	0.465
Fine sand	85.80	1.59	2.35	2.01	0.417
Medium-fine sand	26.70	1.96	1.66	2.57	0.927
Coarse sand	27.80	1.90	1.84	2.74	0.928
High plastic clay	75.80	1.58	2.51	2.26	0.489
Silty sand	79.90	1.54	3.15	2.70	0.529
Silty mud	131.40	1.39	4.43	2.66	0.368

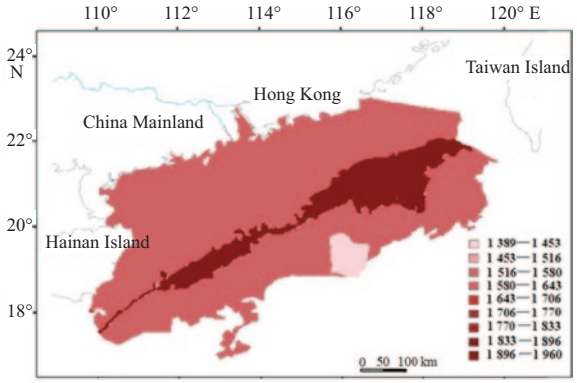

Fig.6. Marine sediment bulk density (mg/cm^3) distribution.

γ'/γ, this paper calculated the relationship of γ'/γ (at a depth of 2.5 m in piston cores) with the values of the bulk density at 10 cm depth. The formula is as follows:

$$\gamma'/\gamma = 0.051 e^{1.115\rho}, \quad (2)$$

where the correlation coefficient square r^2 is 0.801 8; and ρ is the bulk density at 10 cm depth, see Fig. 7.

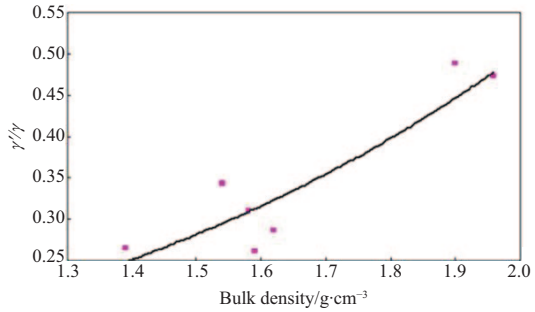

Fig.7. Relationship curve of bulk density with the ratio (γ'/γ) of mean buoyant unit mass to mean total unit one.

3.4 *Northern seismic activity of South China Sea*

The recording time of the northern seismic data is short in the South China Sea, and the recording data are relatively few. In 16°–24°N, 110°–122°E, northern earthquake (M>3) numbers in South China Sea are 501 from 1990 to 2008, focal depth between 5 and 15 km, the earthquake cycle in 0.1–0.2 s (from China Earthquake Networks Center (CENC)).

Among them, the earthquake numbers of M equaling 3–4, 4–5, 5–6 and 6–7 are 391, 89, 20 and 1 respectively, the focal depth 10 km (Fig. 8). History earthquakes (M>7) happened near the South China Sea as follows: (1) M=7 (23.2°N, 117.3°E) in 1600; (2) M=8 in Quanzhou (24.8°N, 119°E) in 1604; (3) M=7.25 at the coast (24.4°N, 118.5°E) in Xiamen in 1906; (4) M=7.5 in Nan'ao (23.2°N, 117.3°E) in 1918 (Xu et al., 2006; Chen et al.,2009).

The northern earthquake activities in the South China Sea are mainly distributed in the continental shelf, continental slope line near the slope area. The earthquakes present a zonal distribution and a cyclic activity. The active and quiet periods

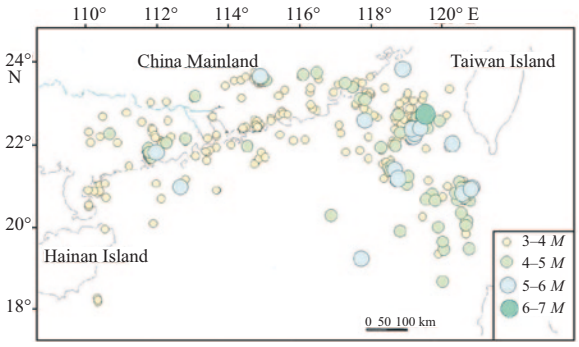

Fig.8. Northern earthquake epicenter in the South China Sea (from the CENC).

alternately emerged (Chen et al., 2009). One seismic belt shows the NEE direction along the northern margin of the South China Sea, and another strong earthquake belt is located to the west edge in the Taiwan Strait.

Approximately, 30% earthquakes occurred in the same area that is closely related to the northern marginal seismic belt, which have a potential danger to coastal engineering in this area. Peak seismic acceleration values can be formatted as a continuous GIS layer (Fig. 9). This paper has used the peak seismic acceleration as a driving stress and formed another environment load condition that leads to the slope instability.

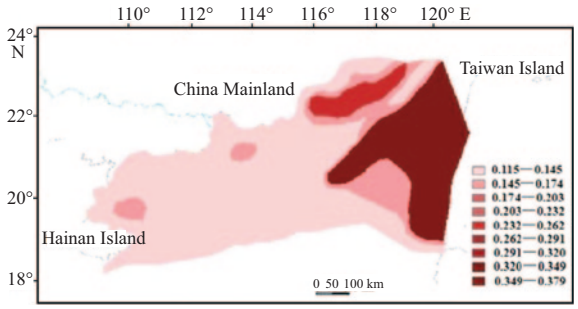

Fig.9. Peak seismic acceleration (m/s^2) with a 10% probability of exceedance in 50 a on the northern continental slope (Chen et al., 2009).

3.5 *Shear stress caused by cyclic load effect*

A seismic load is a key factor to the submarine slope failure, and two factors should be considered during evaluating a shear stress: (1) due to short duration of the earthquakes, the pore water flow does not occur (undrained loading) while most of the damage happen; and (2) seismic cyclic load will cause the pore water pressure increase or decrease, at the same time, a shear strength would change. If using a cyclic, undrained triaxial test to evaluate the strength, the two factors should be considered. The equivalent cyclic shear stress ratio caused by earthquake motion in the sediment layer is r_{cs} (Lu et al., 2005), and it can be calculated according to the following formula:

$$r_{cs} = 0.65 \frac{\alpha_{max}}{g} \frac{\sigma_v}{\sigma'_v} r_d, \quad (3)$$

where α_{max} is the peak acceleration of ground motion; g is gravity acceleration; σ_v is the vertical stress; σ'_v is the vertical effective stress; and r_d is stress reduction factor.

For different depths (z) in sediment, Liao and Whitman (1986) put forward that the stress reduction factors (r_d) could be expressed in the following formula:

$$z \leqslant 9.15 \text{ m},\ r_d = 1.0 - 0.007\,65\,z, \quad (4)$$

$$23 \text{ m} \geqslant z > 9.15 \text{ m},\ r_d = 1.174 - 0.026\,7\,z, \quad (5)$$

$$30 \text{ m} \geqslant z > 23 \text{ m},\ r_d = 0.757 - 0.008\,57\,z. \quad (6)$$

The sediment destruction is usually reflected by the cyclic shear stress ratio and the number of cycles. If a series of samples with the same lithology is tested by different levels of the cyclic shear stress ratio, their shear strengths show an approximate linear relationship. Seed and Idriss (1971) pointed out that the number of a typical representative strong earthquake is an approximation to 10. Accordingly, this paper chooses the point at which cyclic shear stress ratio corresponds to damage in ten cycles as being an approximate measure of cyclic shear strength in the seismically active areas.

By a layer analysis cyclic shear stress ratio is roughly 0.158–0.933 (Fig. 10), which is mainly depending on the initial water content in the marine sediment. For saturated marine sediments, the water content and the bulk density are directly related to the soil particle characteristic.

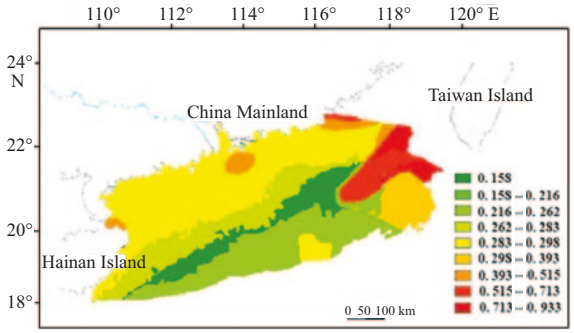

Fig.10. Cyclic shear stress ratio.

When the continental slope is destroyed under the earthquake load, the shear stress (τ_s) caused by an earthquake is approximately equal to the cyclic shear strength. For normal consolidation soil, $\tau_s / \gamma' h = r_{cs}$. The r_{cs} is substituted into Eq. (1), as follows:

$$k_c = (\gamma' / \gamma)(r_{cs} - \sin\alpha)\ , \quad (7)$$

where, k_c is the critical horizontal seismic acceleration required to cause failure.

If the cyclic shear stress ratio is expressed as a function of the sediment bulk density, k_c would be expressed as a function of the sediment bulk density and the continental slope angle, too. When each parameter in Eq. (7) is represented by a map layer, then the GIS's spatial algebra can be used to evaluate the critical horizontal seismic acceleration. The cyclic shear stress ratio and the critical horizontal seismic acceleration can be summarized description in the GIS map (Figs 10 and 11).

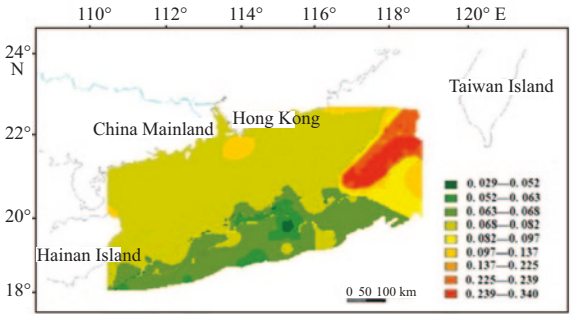

Fig.11. Critical horizontal seismic acceleration (m/s^2).

In fact, the ratio ($\frac{k_c}{a_{max}}$) between the critical horizontal seismic acceleration and the peak seismic acceleration with a 10% probability of exceedance in 50 a on the northern continental slope in the South China Sea is a measure value which is related to a seismically induced slope failure likelihood. The lower values of the ratio represent a greater susceptibility to failure during seismic loading. Applying GIS spatial analysis technology function, this article formed the ratio diagram. The ratio is between 0.25 and 1.03, as shown in Fig. 12. Finally, this continental slope stability map is presented in Fig. 12 by nine different colours.

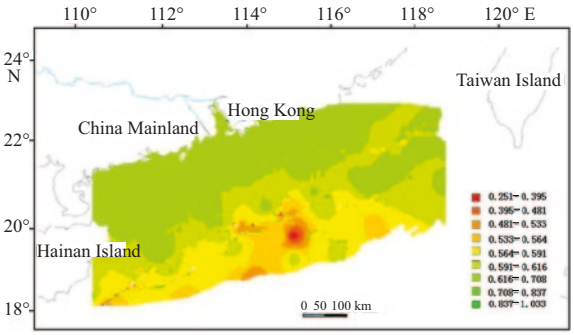

Fig.12. Ratio of the critical horizontal seismic acceleration to the peak seismic acceleration, and continental slope stability map.

4 Conclusions

(1) The upper slope is on the northwest of continental slope, north of 20°30'N, and in the vicinity of 118°E, and the bottom slope angle is bigger, where the slope value is up to 1.938. The middle slope is in the west area of 118°E, gentle terrain, the slope gradient is only 1.301, the slope is relatively flat. The lower slope has long submarine canyons which show the S-N direction, near 20°N and 115°E, where the terrain changes fiercely, the slope value is up to 5.579.

(2) On the northern continental slop, seabed sediments can be classified into seven types: clay, fine sand, medium-fine sand, coarse sand, high plastic clay, silty sand and silty mud.

The seabed sediment particle size increases gradually from the N-W to S-E directions. It shows that sedimentary characteristic law of the seabed deposition is contrary to the general.

(3) This paper has calculated the relationship of the γ'/γ of 2.5 m deep drilling with the density of 10 cm depth being $\gamma'/\gamma = 0.051\mathrm{e}^{1.115\rho}$, .

(4) The equivalent cyclic shear stress ratio is roughly between 0.158 and 0.933, which is mainly depending on the initial water content in the marine sediment. For saturated marine sediments, the water content and the bulk density are directly related to the soil particle characteristic.

(5) The ratio $\frac{k_c}{a_{max}}$ is between 0.25 and 1.03. The unstable regions are mainly distributed along the S-N direction valley (19.5N°, 115.5°E) in lower slope, and the stability is gradually enhanced from the S-E direction to N-W directions.

(6) Contrasting the continental slope stability map with the gradient map, the seabed sediment distribution map and the peak seismic acceleration diagram, respectively, this paper has shown the continental slope stability mainly controlled by a topography fluctuation.

References

Alexander C R, Simoneau A M. 1999. Spatial variability in sedimentary processes on the Eel continental slope. Mar Eol, 154(1–4): 243–254

Chen Renfa, Kang Ying, Huang Xinhui, et al. 2009. Seismic risk analysis in northern South China Sea. South China Journal of Seismology (in Chinese), 29(4): 36–45

Lambe T W, Whitman RV. 1969. Soil Mechanics. New York: Wiley, 553

Lee H J, Edwards B D. 1986. Regional method to assess offshore slope stability. Geotech Eng, 112(5): 489–509

Lee H, Locat J, Dartnell P, et al. 1999. Regional variability of slope stability: application to the Eel margin, California. Marine Geology, 154(1–4): 305–321

Liao S S C, Whitman R V. 1986. Overburden correction factors for SPT in sand. Journal of Geotechnical Engineering, 112(3): 373–377

Liu Zhongchen, Liu Baohua. 2005. China Offshore Topography and Adjacent Waters (in Chinese). Beijing: China Ocean Press, 180–224

Lu Tinghao, Liu Zude, Yin zongze, et al. 2005. Advanced Soil Mechanics (in Chinese). Beijing: Mechanical Industry Press, 300

Luan Xiwu, Peng Xuechao, Qiu Yan. 2009. The structure of the high speed deposit formation in north slope of the South China Sea. Geoscience (in Chinese), 23(2): 183–198

Luan Xiwu, Peng Xuechao, Wang Yingmin, et al. 2010. Sea sand wave characteristics and properties in South China Sea continental shelf. Journal of Geology (in Chinese), 84(2): 233–244

Maslin M, Naja M, Bilal H, et al. 1998. Sea-level and gas hydrate controlled catastrophic sediment failure of the Amazon Fan. Geology, 26(12): 1107–1110

Morgenstern N R. 1967. Submarine slumping and the initiation of turbidity currents. In: Richards A, Ed. Marine Geotechnique. Urbana: University of Illinois Press, 189–210

Rothwell R G, Thomson J, Kähler G. 1998. Low-sea-level emplacement of a very large Late Pleistocene “megaturbidite” in the western Mediterranean Sea. Nature, 393(6674): 377–380

Seed H B, Idriss I M. 1971. Simplified procedure for evaluating soil liquefaction potential. Soil Mech Found Eng Div, 97(9): 1249–1273

Song Haibin. 2003. The study of the dynamic evolution system of natural gas hydrate (Ⅱ): Submarine landslide. Progress in Geophysics (in Chinese), 18(3): 503–511

Wu Shiguo, Chen Shanshan, Wang Zhijun, et al. 2008. Submarine landslide and risk evaluation on its instability in the deepwater continental margin. Geoscience (in Chinese), 22(3): 430–436

Xu Huilong, Qiu Xuelin, Zhao Minghui, et al. 2006. The crustal structure features and epicenter construction of Nan’ao earthquake (M=7.5) in northeast of South China Sea. Science Bulletin (in Chinese), 11(S2): 83–90

Zhang Fuyuan, Zhang Weiyan, Zhang Xiaoyu, et al. 2010. Indices of classification and nomenclature for deep-sea sediment and principal component analysis. Acta Oceanologica Sinica, 32(6):118–129

Zou Dapeng, Lu Bo, Yan Pin, et al. 2012. The temperature change of the three types of sound velocity in the north of the South China Sea seabed sediments. Journal of Geophysics (in Chinese), 55(3): 1017–1024